

RFA-Cut: Semi-automatic Segmentation of Radiofrequency Ablation Zones with and without Needles via Optimal s-t-Cuts

Jan Egger^{1,2,3,4}, Harald Busse⁵, Philipp Brandmaier⁵, Daniel Seider⁵, Matthias Gawlitza⁵
Steffen Stroocka⁵, Philip Voglreiter¹, Mark Dokter¹, Michael Hofmann¹, Bernhard Kainz⁶
Xiaojun Chen⁷, Alexander Hann⁸, Pedro Boechat¹, Wei Yu¹, Bernd Freisleben², Tuomas Alhonnoro³
Mika Pollari³, Michael Moche⁵, Dieter Schmalstieg¹

¹Institute for Computer Graphics and Vision, Graz University of Technology, Austria

²Distributed Systems Group, Philipp University of Marburg, Germany

³School of Science, Aalto University, Espoo, Finland

⁴BioTechMed-Graz, Austria

⁵Dept. of Diagnostic and Interventional Radiology, Leipzig University Hospital, Germany

⁶Dept. of Computing, Imperial College London, UK

⁷School of Mechanical Engineering, Shanghai Jiao Tong University, Shanghai, China

⁸Dept. of Internal Medicine and Gastroenterology, Katharinenhospital, Stuttgart, Germany

Abstract— In this contribution, we present a semi-automatic segmentation algorithm for radiofrequency ablation (RFA) zones via optimal s-t-cuts. Our interactive graph-based approach builds upon a polyhedron to construct the graph and was specifically designed for computed tomography (CT) acquisitions from patients that had RFA treatments of Hepatocellular Carcinomas (HCC). For evaluation, we used twelve post-interventional CT datasets from the clinical routine and as evaluation metric we utilized the Dice Similarity Coefficient (DSC), which is commonly accepted for judging computer aided medical segmentation tasks. Compared with pure manual slice-by-slice expert segmentations from interventional radiologists, we were able to achieve a DSC of about eighty percent, which is sufficient for our clinical needs. Moreover, our approach was able to handle images containing (DSC=75.9%) and not containing (78.1%) the RFA needles still in place. Additionally, we found no statistically significant difference ($p < 0.423$) between the segmentation results of the subgroups for a Mann-Whitney test. Finally, to the best of our knowledge, this is the first time a segmentation approach for CT scans including the RFA needles is reported and we show why another state-of-the-art segmentation method fails for these cases. Intraoperative scans including an RFA probe are very critical in the clinical practice and need a very careful segmentation and inspection to avoid under-treatment, which may result in tumor recurrence (up to 40%). If the decision can be made during the intervention, an additional ablation can be performed without removing the entire needle. This decreases the patient stress and associated risks and costs of a separate intervention at a later date. Ultimately, the segmented ablation zone containing the RFA needle can be used for a precise ablation simulation as the real needle position is known.

I. INTRODUCTION

Mainly because of hepatitis infections and alcohol abuse, liver cancer is on the rise worldwide. Especially patients with Hepatocellular Carcinomas (HCC) have a poor prognosis because of its late symptomatic onset resulting in a median survival time of four to six months from the time of diagnosis when untreated. However, according to the recent treatment guidelines [1], Radiofrequency ablations (RFA) serve as a first

line therapy approach for early HCC in patients with liver cirrhosis. In addition, the local usage of ablation therapies increases for metastatic liver disease. Originally developed for patients who were not eligible for surgery, the usage has now expanded to patients as a bridge to liver transplantation and even as an alternative to surgical resection in the early stages of the disease [2]. In the early 1990s, RFA was first described followed by huge technical advances throughout the last decades. In summary, the underlying principle is based on a high frequency alternating current which is delivered through one or more electrodes placed inside the lesion [3] (Fig. 1).

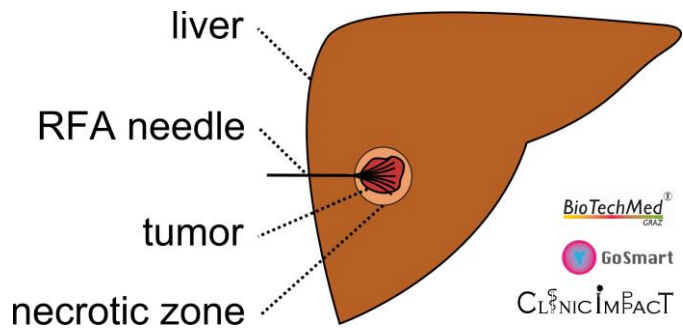


Fig. 1. Sketch of a liver (brown) with an umbrella-shaped and fully expanded radiofrequency ablation (RFA) needle in black. The needle tips are located inside a liver tumor (red) which is surrounded by the necrotic zone (light brown).

The heat that is generated around the electrodes destroys the cancer cells by inducing a coagulative necrosis as a result of denaturation of cellular proteins. In general, tissue necrosis already begins at approximately 60°C, but in general, temperatures over 100° are needed to achieve satisfying results. Also the placement of the needle and the individual impedance determine the amount of destroyed tissue. Further, it is inversely proportional to the square of the distance from the electrode, and as a result, tissue cools rapidly away from the tip of the needle probe. Thus, the proximity to large blood vessels plays also a major role in the heat transmission.

Normally, the blood flow protects the vessel wall from getting damaged, however, on the flipside acts as a heat sink by cooling down nearby tissue limiting the methods overall success [4]. As a consequence, a significant mismatch between expected and truly induced lesion size and geometry has been observed in many liver RFAs. On one side, it can lead to over-treatment with severe injuries (up to 9% major complications [5]) or, on the other side, to under-treatment with tumor recurrence (up to 40% [5]). Cohort patient studies have shown the evidence of a significant reduction in the recurrence rate, if there is a safety rim generated around the tumor via the RFA [6]. This elicits the need for (1.) a reliable method for the comparison of localization, geometry and size of the tumor in the preoperative images, and (2.) a thermally induced lesion after ablation. Tumor recurrence can be diagnosed by the detection of typical alteration in tissue enhancement, but an increase of the size or a change of the geometry of the lesion seems to be a more sensitive indicator of early recurrence in follow-up imaging. Thus, a reliable and feasible determination of the ablation zone at baseline and follow-up may contribute to a positive outcome for the patient and can therefore lead to a better understanding of the cause of new tumor growth. And the additional knowledge might lead to an improvement of ablation protocols or even in the long term to new treatment strategies. However, the determination of therapeutically induced lesions after minimally invasive cancer treatment can be performed by segmentation, which is usually done by a very time consuming manual (slice-by-slice) procedure – and thus not yet part of the clinical routine. But a validated segmentation algorithm may have the potential to increase the acceptance of the method in the medical community and finally lead to a benefit in patient treatment. The overall segmentation (and partially also registration) field in Computer Vision deals with the computer-aided analysis and classification of image data in a broad range of applications [7]-[19]. This can be the automatic detection of humans in videos [20] or the volumetry of brains from medical images [21]. The aim of a segmentation algorithm is mainly to support and speedup a time-consuming manual selection and contouring process. In the literature, a number of algorithms have been proposed, like Active Contours (ACM) [22]-[25], Deformable Models [26]-[32], Active Appearance Models (AAM) [33]-[36], graph-based approaches [37]-[40], fuzzy-based approaches [41], or neural networks [42], which often base on a mathematical model from another discipline, like Physics or Electrical Engineering, or a combination of several mathematical models. Furthermore (or alternatively), the segmentation methods can be classified as fully-automatic or semi-automatic algorithms. A research group working in the specific area of (semi-)automatic segmentation of ablation zones in RFA scans of the liver are Passera et al. [43]. They apply a Live-Wire algorithm (implemented within the MeVisLab platform [44], www.mevislab.de) and clustering for the segmentation, but they did not use data where the RFA needle is still present within the scan. However, this is the case when the interventional radiologist (or interventionalist) particularly wants to assess the size of the induced lesion, to check if an additional ablation is needed. And to avoid the repositioning or the replacement of the needle, it remains inside the liver while performing the control scan. In addition, the introduced segmentation method worked only in 2D, which can be very time-consuming in case of tumors or

ablation zones that extend over many slices and the reported segmentation time was ten minutes. McCreedy et al. [45] presented another 2D livewire-based method, a radio frequency ablation registration, segmentation, and fusion tool called RFAST. However, the (segmentation) process has not been described in detail and no quantitative segmentation results have been presented. Keil et al. [46] presented the semi-automated segmentation of liver metastases treated by radiofrequency ablation with an algorithm that consists of six steps including a three-dimensional region growing and morphologic operations, like erosion, dilation. In addition, the user has to draw a diameter across larger lesions or provide a single click inside smaller lesion as initialization. A workflow oriented software support for image guided RF ablations of focal liver malignancies has been introduced by Weihusen et al. [47]. Thereby, they also segment coagulation necrosis in the – post-interventional – control scans (after the ablation). After the user has provided a seed point inside the ablation zone, a morphology-based region growing algorithm is started, which has been proposed by Kuhnigk et al. [48]. Finally, the user has the option to correct the segmentation outcome towards more “irregular” or “roundish” geometry by manual interaction. Initial results of a 3D shape-based analysis of CT acquisitions for the detection of local recurrence of liver metastases after RFA treatment, have been reported by Bricault et al. [49]. In doing so, they applied a semi-automated 3D segmentation method that uses a “tagged” watershed algorithm. On average, the segmentation process took about four minutes and the minimum required user interaction included two mouse clicks: the first one in the ablated tumor and the second one in the surrounding liver parenchyma. Elsewhere, Stippel et al. [50] introduced a volumetric evaluation study of the variability of the size and the shape of necrosis that have been induced by RF ablations in human livers. Therefore, the study has been performed with the software package VA 40C from Siemens on a Leonardo workstation. For the overall segmentation process of the ablation-induced lesions, a region of interest had to be defined in each slice by manually tracking the approximate lesion borders. Then, the precise border of the lesion was determined by a filter algorithm from the software package, which was based on density differences between the ablated and the liver tissue. In addition to this section, we want to point the interested reader to a state of the art publication about computer-assisted planning, intervention and assessment of liver tumor ablation from Schumann et al. [51].

Finally, to the best of our knowledge, there is no work that has studied the semi-automatic 3D segmentation of post-interventional RF ablation zones with clinical data that has the ablation needles still in place.

II. MATERIAL AND METHODS

A. Data Acquisition

We used twelve datasets from ten patients, who underwent radiofrequency ablation in the liver, for this retrospective study [52], [53]. The number of slices in z direction ranged from 52 to 232 and all datasets had a matrix size of 512x512 in x- and y-direction. The slice thickness was either one or two mm, and the pixel spacing ranged from 0.679 to 0.777, with spacing between the slices of one to three mm. The ablation needle was still present in six datasets, and all datasets have been acquired on multislice CT scanner (Philips Brilliance or Mx8000,

Philips Healthcare, Netherlands). The data analysis and publication, was approved by the Institutional Review Board (IRB) of the Leipzig University Hospital under the reference number: 381-14-15122014. In addition, we plan to provide the datasets to the research community on our ClinicImpact project page:

<http://www.clinicimpact.eu/>

Medical ablation datasets from a comprehensive pig study can already be found on the webpage of our European Project named *GoSmart* [54]:

<http://www.gosmart-project.eu/>

B. Manual Segmentation

The Ground Truth of the ablation zones has been generated by setting up a simple segmentation framework for manual contouring under MeVisLab. This allowed the physicians to manually outline the RFA lesions slice-by-slice without any algorithmic support (to avoid distortions). Then, the single contours were voxelized and merged to a 3D mask, which represented the manual segmented ablation zone. Afterwards, the 3D masks were used for comparison and quantitative evaluation with the RFA-Cut segmentation results.

C. Evaluation Metric

For evaluation we used the Dice Similarity Coefficient (DSC) metric [55]-[58], widely used in medical image analysis and describing the agreement between two binary volumes M and S :

$$DSC = \frac{2 \cdot V(M \cap S)}{V(M) + V(S)} \quad (1)$$

M and S are the binary masks from the manual (M) and the semi-automatic RFA-Cut (S) segmentations, $V(\cdot)$ denotes the volume (in cm^3) and \cap denotes the intersection. The volume was computed by counting the number of voxels and multiplying them with the physical size of voxels. However, in addition to the DSC, we measured also the time it took an experienced radiologist to manually outline the ablation zones and compared it with the computation time of the semi-automatic RFA-Cut segmentations.

D. Semi-automatic Segmentations with the RFA-Cut

The semi-automatic segmentation algorithm named RFA-Cut uses a spherical template to set up a three-dimensional graph $G(V, E)$ around the ablation zone [59]. Altogether, the Graph G consists of nodes $n \in V$ and edges $e \in E$ connecting these nodes, and a source s and a sink t [60]-[63]. The nodes n are sampled along rays whose origin resides at the user-defined seed point (inside the image), while their direction points towards the surface of a polyhedron [64]. After the graph has been constructed (for more details please see [65]-[69] and its origin for aorta segmentation and stent simulation [70]-[79]), the segmentation result is calculated by dividing the graph into two sets of nodes via a Min-Cut/Max-Flow algorithm [80]. In doing so, one set of nodes represents the ablation zone (called foreground) and the other set represents the surrounding structures (called background). Note that the basic segmentation scheme has already been successfully applied to pituitary adenomas [81] and prostate central glands [82].

However, the *rigid* segmentation scheme was later turned into an interactive real-time approach [83]-[87], and for this study it was enhanced by an additional refinement option [88]-[91]. To initialize the interactive segmentation process, the user has to place only one seed point roughly in the middle of the ablation zone on a 2D slice of the (CT) scan (note: the segmentation, however, performs in 3D). From the seed point position, the graph is generated in the background (not visible to the user) and segmentation result is automatically calculate (min-cut) and displayed to the user in 2D and 3D views. Nevertheless, the user can drag the seed point around to interactively generate new segmentation results, which always depend on the new/current seed point positions. Moreover, the user can drop the seed point (by means it remains at a fixed position in the image) and add an arbitrary amount of additional seed points along the border of the ablation zone. In doing so, the algorithm gets additional input about the location of the border and steers the behavior of the min-cut. Though, the user can always come back to the initial seed point, grab it and start dragging it around the image again. Note that the additional placed seed points along the ablation boarder will not get lost then, they stay fixed and continue to influence/restrict the min-cut calculation. The schematic workflow of the RFA-Cut is shown in Fig. 2.

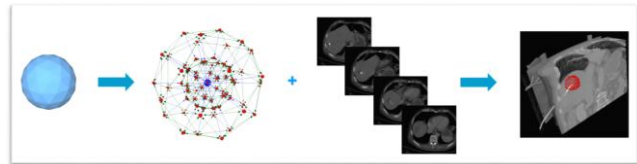


Fig. 2. Schematic workflow of the RFA-Cut segmentation: a sphere (left, blue) is used to construct a graph (second image from the left). Then, the graph is constructed (note: not visible to the user) at the user-defined seed point position within the image (third image from the left). Finally, the segmentation result of the RFA-Cut (red) corresponding to the current seed point is shown to the user (rightmost image).

III. RESULTS

Our proposed interactive segmentation algorithm RFA-Cut has been implemented as an own C++ module (under Microsoft Visual Studio 2008) for the medical prototyping platform MeVisLab. The overall computation of the segmentation result – including the graph construction from the current user-defined seed point position and the optimal min-cut calculation – could be performed within one second on a laptop (with Intel Core i5-750 CPU, 4×2.66 GHz, 8 GB RAM, Windows 7 Professional x64 Version with Service Pack 1 installed). As a consequence, this enabled real-time feedback of our algorithm presented to the user and the immediate response and feedback of the segmentation allowed user guidance of the algorithm to a satisfying outcome.

Fig. 3. shows the result of a semi-automatic segmentation of a post-interventional ablation zone for visual inspection. Because the computed tomography (CT) data has been acquired immediately after the treatment, the ablation needle is still in place and thus visible in the scan. The image on the left shows the axial slice with a user-defined seed point (blue) and the red dots are the border of the segmentation in this slice (note: these dots represent the last nodes of the graph that are still bound to the source s after the min-cut calculation). The

image in the middle shows the segmentation result in a 3D view, and the red dots show the last nodes of the graph which are still connected to the source after executing the min-cut calculation. The rightmost image presents a closed surface in green, which represents the segmentation result, and that has been generated from the graph's nodes. Later, this closed surface is used to generate the solid 3D mask for the Dice Similarity Coefficient calculation with a pure manual slice-by-slice segmentation.

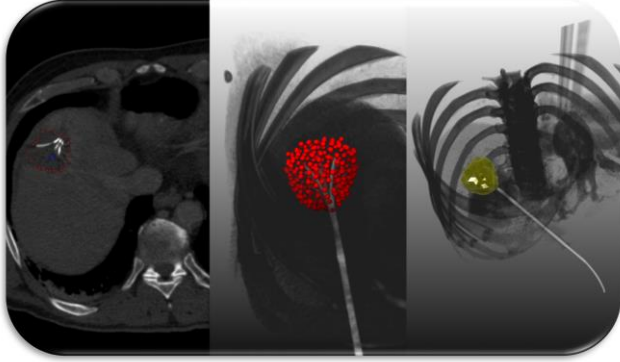


Fig. 3. RFA-Cut segmentation result of an ablation zone in a post-interventional CT scan (still including the ablation needle). The axial slice where the user-defined seed point (blue) has been placed, is shown in the left image. In addition, the corresponding segmentation result (red dots) is presented (note: the red dots are the last nodes of the graph that are still bound to the source s after the min-cut calculation). A 3D view of all nodes (red dots) that describe the surface of the segmented ablation zone after the min-cut calculation is shown in the middle image. Moreover, the rightmost image displays a closed surface (green) of the segmentation result of the RFA-Cut (red dots from the previous image). Finally, the closed surface of the segmentation result is used to generate a solid mask for the DSC calculation.

Table 1 and Table 2 present the direct comparison of manual slice-by-slice segmentations from physician 1 and 2 with RFA-Cut segmentation results for twelve ablation zones using the Dice Similarity Coefficient. In addition, Table 3 presents the direct inter-observer comparison of manual slice-by-slice segmentations from physician 1 and physician 2 via the DSC.

	Volume (cm ³)		Number of Voxel		DSC (%)
	manual 1	semi	manual 1	semi	
	10.0	6.3	5866	3689	71.8
Range	–	–	–	–	–
	122.6	104.0	70806	70208	83.5
μ	35.9	33.0			77.0
\pm	\pm	\pm	31294.8	30756.3	\pm
σ	30.0	25.1			4.7

Tab. 1. This table presents the direct comparison of manual slice-by-slice segmentations from physician 1 and semi-automatic RFA-Cut segmentation results for twelve ablation zones via the DSC.

	Volume (cm ³)		Number of Voxel		DSC (%)
	manual 2	semi	manual 2	semi	
	11.1	6.3	6543	3689	68.1
Range	–	–	–	–	–
	117.7	104.0	67963	70208	85.3
μ	36.2	33.0			77.1
\pm	\pm	\pm	31240.1	30756.3	\pm
σ	28.7	25.1			5.8

Tab. 2. Similar to the first table, this table presents the direct comparison of the RFA-Cut segmentation results with physician 2.

	Volume (cm ³)		Number of Voxel		DSC (%)
	manual 1	manual 2	manual 1	manual 2	
	10.0	11.1	5866	6543	82.4
Range	–	–	–	–	–
	122.6	117.7	70806	67963	92.6
μ	35.9	36.2			88.8
\pm	\pm	\pm	31294.8	31240.1	\pm
σ	30.0	28.7			3.3

Tab. 3. This table presents the direct comparison of the manual slice-by-slice segmentations from physician 1 and physician 2 (from table 1 and table 2) for the twelve ablation zones also via the DSC.

Furthermore, we differentiated between the acquisitions where the RF electrodes were still in place and the cases where the RF electrodes have already been removed. However, we found no significant differences between these cases, and the DSC values between experts were significantly higher ($p < 0.01$) than those between automatic and manual processing (88.8% vs. 77.0%). This was also independent of whether the needle was still included (86.8% vs. 75.9%, $p < 0.05$) in the dataset or not (90.9% vs. 78.1%, $p < 0.05$), respectively. For automatic processing the segmented volumes appeared to be smaller than for experts (33.03 ml vs 36.02 ml), but the differences were not statistically significant: $p = 0.308$. This was also the case for scans with the needle included (25.76 ml vs. 25.93 ml, $p = 0.917$) and without (40.30 ml vs. 46.10 ml, $p = 0.249$). The overall mean DSC value of both experts appeared to be smaller when the needle was present (75.9% vs. 78.1% without, $p = 0.423$), however, the difference was not significant. On the other hand, the inter-observer DSC was significantly higher when the needle was not present (90.9% without vs. 86.8%, $p = 0.025$). The statistical differences in the DSC values and segmentation volumes between the methods were analyzed with Wilcoxon signed-rank tests. And differences between both subgroups (with and without needle present) with a Mann-Whitney test. All analyses were performed with Version 20 of SPSS from IBM (using a level of significance of 0.05). However, in summary, the main difference between the automatic and manual segmentation is the computation time. Making use of the introduced automatic tool, a segmentation could be performed in a few seconds, whereas a pure manual segmentation took on average between 48 seconds and 8 min 16 seconds (mean 3 min 13 seconds).

IV. CONCLUSIONS

Radiofrequency ablations of liver tumors induces areas of tissue necrosis, which can be visualized reliably in contrast enhanced CT scans. In this paper, an interactive segmentation algorithm was applied to routine control CT scans after RFA of liver cancer for the semi-automatic determination of the thermally induced lesions. Semi-automatic segmentation accuracy was found to be sufficient for most of the cases, although a manual slice-by-slice segmentation still provided the best accuracy. However, speed was the main advantage of the proposed tool over manual segmentation, which makes it an appealing alternative for physicians. As stated in the introduction, a minimally invasive RFA can be an alternative to open surgery and might also be suitable for inoperable patients. In addition, when the interventional radiologist presumes that continuing of the therapy might be necessary,

the RFA needle may still reside in the target organ during image acquisition (note that post-interventional imaging is regularly performed to document the success of the RFA treatment). Furthermore, hardening artefacts can compromise the image quality significantly, but such cases were also segmented and included in this study. Manual slice-by-slice segmentations have been performed by two radiological experts for the evaluation of the RFA-Cut; this enabled the DSC calculation between the manual and the semi-automatic RFA-Cut segmentation outcome. In conclusion, the achieved highlights of this publication are:

- Applying an interactive segmentation algorithm to RFA acquisitions from the clinical routine;
- Using post-interventional patient scans with and without RFA needles still in place;
- Clinical experts performed manual slice-by-slice segmentations for an evaluation;
- DSC calculation for a statistical validation of the RFA-Cut;

For a comparison of our employed method with an existing segmentation approach, we applied the GrowCut implementation in (3D) Slicer (www.slicer.org) [92], [93] to our data. This GrowCut implementation is user friendly, because it does not require any precise parameter setting. Rather the user initializes the algorithm by marking areas in the image with several simple strokes (Fig. 4.). Moreover, we've had already good experiences with certain types of brain tumors (Glioblastoma multiforme (GBM) [94] and pituitary adenomas [95]) and vertebral bodies [96]. But especially the cases where the needles were still in place and therefore visible within the images caused segmentation problems (Fig. 5.). In more detail, GrowCut leaks along the needles, because it cannot handle the large gray value differences between the ablation zone (dark) and the RFA needle (bright). In addition, the initialization of GrowCut (marking parts of the lesion and the background) takes a trained user between thirty and sixty seconds, in contrast to our method that needs only a single seed point. Furthermore, the user has to wait several seconds for the GrowCut segmentation result (about ten seconds on the PC we used also for interactive method). In contrast, our method provides the segmentation result immediately, which also makes refinement much more convenient. The sharp edges of the GrowCut segmentation result (green) in the rightmost image of Fig. 5. occur, because the (3D) Slicer implementation restricts the segmentation area with a bounding box – note that the size of the bounding box depends on the manual GrowCut initialization of the user.

There are several areas for future work, like the integration of the interactive segmentation algorithm into a medical application framework for supporting ablation therapies. The framework is currently under development within a project funded by the European FP7 program and is based the continuation on the European project IMPPACT (Image-based Multi-scale Physiological Planning for Ablation Cancer Treatment, grant agreement no. 223877) [97] (<http://www.imppact.eu/>). More precise, we plan to use our semi-automatic algorithm for the segmentation of difficult cases where automatic methods fail. Furthermore, we plan to provide the datasets acquired during the project over the next

years to the public. Finally, we want to investigate the possibilities for liver tumor tracking after one or several RFA interventions and support the needle placement [98] with our real-time segmentation algorithm and motion tracking [99] in an Augmented Reality (AR) setting [100].

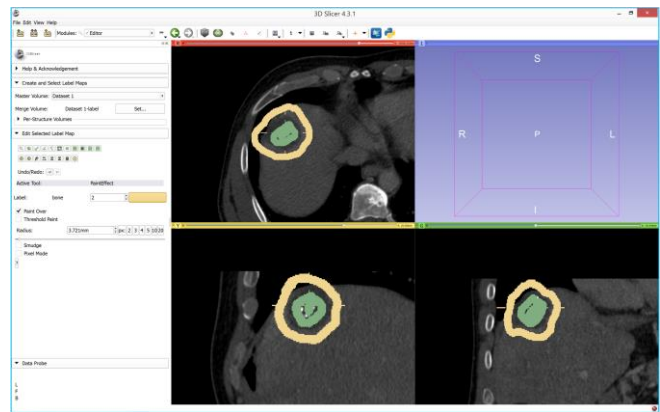


Fig. 4. Manual GrowCut initialization for the segmentation of the RF ablation zone: the ablated zone is marked in green and the background is marked in yellow on three 2D slices, respectively.

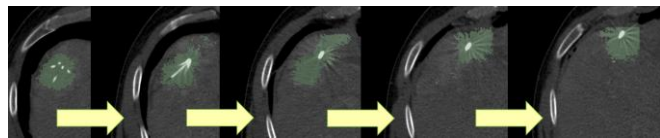


Fig. 5. The GrowCut segmentation result (green) for the manual initializing from Fig. 4. The GrowCut segmentation leaks along the RF ablation needle, because it cannot handle the large gray value differences between the ablation zone (dark) and the needle (bright). The sharp edges of the segmentation result in the rightmost image occur, because the GrowCut implementation under Slicer automatic restricts the segmentation area with a bounding box that depends on the user initialization.

ACKNOWLEDGMENT

The work received funding from the European Union (EU) in FP7: Clinical Intervention Modelling, Planning and Proof for Ablation Cancer Treatment (ClinicIMPACT, grant agreement no. 610886) and Generic Open-end Simulation Environment for Minimally Invasive Cancer Treatment (GoSmart, grant agreement no. 600641). Dr. Xiaojun Chen receives support from NSFC (National Natural Science Foundation of China) grant 81171429 and Dr. Bernhard Kainz is supported by an EU FP7 MC-IEF 325661 grant. Dr. Dr. Jan Egger receives funding from BioTechMed-Graz (“*Hardware accelerated intelligent medical imaging*”). Videos demonstrating the RFA-Cut can be found under the YouTube channel:

<https://www.youtube.com/c/JanEgger/videos>

REFERENCES

- [1] G. Graf, et al., “Multimodal treatment of hepatocellular carcinoma,” *Eur J Intern Med*, Mar 22 2014.
- [2] D. S. Lu, et al., “Percutaneous radiofrequency ablation of hepatocellular carcinoma as a bridge to liver transplantation,” *Hepatology* 41, 1130-1137, 2005.
- [3] E. Buscarini, et al., “Radiofrequency thermal ablation of liver tumors,” *Eur Radiol* 15, 884-894, 2005.

- [4] H. Rhim, et al., "Radiofrequency ablation of hepatocellular carcinoma: pros and cons," *Gut Liver* 4, Suppl 1, 113-8, 2010.
- [5] S. L. Wong, et al., "American Society of Clinical Oncology 2009 clinical evidence review on radiofrequency ablation of hepatic metastases from colorectal cancer," *J Clin Oncol.* 28, 493-508, 2010.
- [6] J. Liu, et al., "Therapeutic efficacy comparison of radiofrequency ablation in hepatocellular carcinoma and metastatic liver cancer," *Exp Ther Med.* 7, 897-900, 2014.
- [7] T. Kapur, et al., "Registration and Segmentation for Image Guided Therapy," *Springer*, 79-91, 2014.
- [8] J. Egger, et al., "Body Landmark Detection for a Fully Automatic AAA Stent Graft Planning Software System," *CBMS*, 364-369, 2010.
- [9] D. Richter, et al., "Tetraoptical Camera System for Medical Navigation," Proceedings of the 17th International EURASIP Conference BIOSIGNAL, Brno, Czech Republic, 270-272, Vutium Press, 2004.
- [10] D. Richter, et al., "An Algorithm for the Determination of the Position of Patients and Biopsy Needles with a Four-Camera System," *BVM*, Springer Press, 316-320, 2006.
- [11] D. Richter, et al., "System for Three-Dimensional Reconstruction of Spatial Point-Models from more than two Fragmented Stereoscopic Pictures for Medical Applications," German Patent Application, DE 102004015498 A1 (DPMA - German Patent and Trade Mark Office), 2004.
- [12] J. Egger, et al., "Fast Self-Collision Detection and Simulation of Bifurcated Stents to Treat Abdominal Aortic Aneurysms (AAA)," *29th Annual International Conference of the IEEE Engineering in Medicine and Biology Society*, Lyon, France, 6231-6234, IEEE Press, 2007.
- [13] T. Kapur, et al., "3-T MR-guided brachytherapy for gynecologic malignancies," *Magn Reson Imaging.* 30(9):1279-90, 2012.
- [14] M. H. A. Bauer, et al., "Boundary Estimation of Fiber Bundles derived from Diffusion Tensor Images," *Int J CARS*, 6(1):1-11, 2011.
- [15] J. Klein, et al., "On the Reliability of Diffusion Neuroimaging," *Neuroimaging*, Sciyo, 1-24, ISBN 978-953-307-127-5, 2010.
- [16] B. Kainz, et al., Adaptive Scan Strategies for fetal MRI Imaging using Slice to Volume Techniques. ISBI: From Nano to Macro, IEEE, 2015.
- [17] G. Pernelle, et al., "Robust Applicator Registration for Interstitial Gynecologic Brachytherapy," *Brachytherapy*, Volume 12, Supplement 1, Page S53, 2013.
- [18] D. Röttger, et al., "GPU-Based Isosurface Calculation for Real-time Ablation Zone Navigation," *Research Disclosure*, ID 591066, Published in the Research Disclosure Journal 7/13, 2013.
- [19] D. Kuhnt, et al., "Fiber tractography based on diffusion tensor imaging (DTI) compared with High Angular Resolution Diffusion Imaging (HARDI) with compressed sensing (CS) – initial experience and clinical impact," *Neurosurgery*, Volume 72, pp. A165-A175, 2013.
- [20] A. O. Neeti, "Survey of Techniques for Human Detection from Video," M.S. Scholarly paper, *University of Maryland*, pp. 1-15, 2005.
- [21] R. A. Heckemann, et al., "Automatic volumetry on MR brain images can support diagnostic decision making," *BMC Med Imaging.* 8:9, 08.
- [22] M. Kass, et al., "Snakes - Active Contour Models," *International Journal of Computer Vision* 1, 321-331, 1987.
- [23] J. Lu, et al., "Segmentation and Visualization of Lumen and Thrombus of Thoracic Aortic Aneurysm," *CURAC*, 251-254, 2007.
- [24] S. Großkopf, et al., "Method for Processing Medical Image Data," German Patent Application, DE 102007045268 A1 (DPMA - German Patent and Trade Mark Office), Siemens AG, April 2009.
- [25] J. Lu, et al., "Detection and Visualization of Endoleaks in CT Data for Monitoring of Thoracic and Abdominal Aortic Aneurysm Stents," *SPIE Med Img* 6918, 69181F(1-7), 2008.
- [26] T. McInerney, et al., "Deformable models in medical image analysis: a survey," *Medical Image Analysis* 1, 91-108, 1996.
- [27] D. Zukić, et al., "Segmentation of Vertebral Bodies in MR Images," *Vision, Modeling, and Visualization*, 135-142, 2012.
- [28] D. Zukić, et al. "Robust Detection and Segmentation for Diagnosis of Vertebral Diseases using Routine MR Images," *Computer Graphics Forum*, Volume 33(6), 190-204, 2014.
- [29] D. Zukić, et al., "Glioblastoma Multiforme Segmentation in MRI Data with a Balloon Inflation Approach," *RBC*, 9-13, 2010.
- [30] J. Egger, et al., "A Comparison of Two Human Brain Tumor Segmentation Methods for MRI Data," *RBC*, 40-44, 2010.
- [31] D. Zukić, et al., "Preoperative Volume Determination for Pituitary Adenoma," *SPIE*, Vol. 7963, pp. 79632T-79632T-7, 2011.
- [32] J. Egger, et al. "Segmentation of Pituitary Adenoma: A Graph-based Method vs. a Balloon Inflation Method," *Comput Methods Programs Biomed.*, 110(3), 268-78, 2013.
- [33] T. F. Cootes, et al., "Active Appearance Models," *Proceedings of the European Conference on Computer Vision* 2, 484-498, 1998.
- [34] T. F. Cootes, et al., "Active Shape Models - Smart Snakes," *Proceedings of the British Machine Vision Conference*, 266-275, 1992.
- [35] T. F. Cootes, et al., "Statistical Models of Appearance for Computer Vision," Technical report, *University of Manchester*, 2004.
- [36] K. Greiner, et al., "Segmentation of Aortic Aneurysms in CTA Images with the Statistic Approach of the Active Appearance Models," *Proceedings of Bildverarbeitung für die Medizin (BVM)*, Berlin, Germany, Springer Press, pp. 51-55, 2008.
- [37] J. Shi, et al., "Normalized cuts and image segmentation," *IEEE Transactions on Pattern Analysis and Machine Intelligence* 22, 888-905, 2000.
- [38] M. H. A. Bauer, et al., "A fast and robust graph-based approach for boundary estimation of fiber bundles relying on fractional anisotropy maps," *20th International Conference on Pattern Recognition (ICPR)*, Istanbul, Turkey. IEEE Computer Society, Los Alamitos, 4016-4019, 2010.
- [39] M. H. A. Bauer, et al., "Ray-Based and Graph-Based Methods for Fiber Bundle Boundary Estimation," *Biosignal*, Paper-ID: 048:1-4, 2010.
- [40] M. H. A. Bauer, et al., "A Semi-Automatic Graph-Based Approach for Determining the Boundary of Eloquent Fiber Bundles in the Human Brain," *DGBMT*, Band 55, Heft s1, 123-126, 2010.
- [41] Z. X. Ji, et al., "A modified possibilistic fuzzy c-means clustering algorithm for bias field estimation and segmentation of brain MR image," *Comput Med Imaging Graph.* 35, 383-97, 2011.
- [42] J. C. Fu, et al., "Image segmentation by EM-based adaptive pulse coupled neural networks in brain magnetic resonance imaging," *Comput Med Imaging Graph.* 34, 308-20, 2010.
- [43] K. Passera, et al., "Radiofrequency ablation of liver tumors: quantitative assessment of tumor coverage through CT image processing," *BMC Medical Imaging*, 13, 2013.
- [44] J. Egger, et al., "Integration of the OpenIGTLink Network Protocol for Image-Guided Therapy with the Medical Platform MeVisLab," *Int J Med Robot.* 8(3):282-90, 2012.
- [45] E. S. McCreedy, et al., "Radio frequency ablation registration, segmentation, and fusion tool," *IEEE Trans Inf Technol Biomed.* 10, 490-6, 2006.
- [46] S. Keil, et al., "Semiautomated versus manual evaluation of liver metastases treated by radiofrequency ablation," *J Vasc Interv Radiol.* 21, 245-51, 2010.
- [47] A. Weihusen, et al., "Workflow oriented software support for image guided radiofrequency ablation of focal liver malignancies," *Proc. of the SPIE Medical Imaging*, 6509, article id 650919, 2007.
- [48] J. Kuhnigk, et al., "Fast automated segmentation and reproducible volumetry of pulmonary metastases in CT-scans for therapy monitoring," *Proc. of MICCAI*, 3217, 933-941, 2004.
- [49] I. Bricault, et al., "Liver metastases: 3D shape-based analysis of CT scans for detection of local recurrence after radiofrequency ablation," *Radiology* 241, 243-50, 2006.
- [50] D. Stippel, et al., "Variability of size and shape of necrosis induced by radiofrequency ablation in human livers: a volumetric evaluation," *Ann Surg Oncol.* 11, 420-5, 2004.
- [51] C. Schumann, et al., "State of the art in computer-assisted planning, intervention, and assessment of liver-tumor ablation," *Crit Rev Biomed Eng.* 38, 31-52, 2010.
- [52] H. F. Busse, et al., "Novel Semiautomatic Real-time CT Segmentation Tool and Preliminary Clinical Evaluation on Thermally Induced Lesions in the Liver," *100th RSNA*, PHS 171, December 2014.
- [53] J. Egger, et al., "Semi-automatic Segmentation of Ablation zones in post-interventional CT Data," *BVM*, Springer, 281-286, 2015.
- [54] B. Kainz, et al., "High-Resolution Contrast Enhanced Multi-Phase Hepatic Computed Tomography Data from a Porcine Radio-Frequency Ablation Study," *IEEE ISBI*, Beijing, China, 2014.
- [55] K. H. Zou, et al., "Statistical Validation of Image Segmentation Quality Based on a Spatial Overlap Index: Scientific Reports," *Academic Radiology*, 11(2), 178-189, 2004.
- [56] M. P. Sampat, et al., "Measuring intra- and inter-observer agreement in identifying and localizing structures in medical images," *IEEE Inter Conf Image Processing*, 4 pages, 2006.

- [57] K. G. Baum, et al. "Application of the Dice Similarity Coefficient (DSC) for Failure Detection of a Fully-Automated Atlas Based Knee MRI Segmentation Method," *ISMRM Annual Meeting*, 2010.
- [58] L. R. Dice, "Measures of the Amount of Ecologic Association between Species," *Ecology*, vol. 26, 297-302, 1945.
- [59] J. Egger, et al., "Nugget-Cut: A Segmentation Scheme for Spherically- and Elliptically-Shaped 3D Objects," *DAGM 6376*, 383-392, 2010.
- [60] K. Li, et al., "Optimal Surface Segmentation in Volumetric Images - A Graph-Theoretic Approach," *IEEE Transactions on Pattern Analysis and Machine Intelligence (PAMI)*, 28(1), 119-134, 2006.
- [61] K. Li, et al., "Efficient Optimal Surface Detection: Theory, Implementation and Experimental Validation," *Proc. SPIE Int'l Symp. Medical Imaging: Image Processing*, vol. 5370, 620-627, 2004.
- [62] K. Li, et al., "Globally Optimal Segmentation of Interacting Surfaces with Geometric Constraints," *Proc. IEEE CS Conf. Computer Vision and Pattern Recognition (CVPR)*, vol. 1, 394-399, 2004.
- [63] X. Wu, et al., "Optimal Net Surface Problems with Applications," *Proceedings of the 29th International Colloquium on Automata, Languages and Programming (ICALP)*, 1029-1042, 2002.
- [64] J. Egger, et al., "A Fast Vessel Centerline Extraction Algorithm for Catheter Simulation," *CBMS*, 177-182, IEEE Press, June 2007.
- [65] J. Egger, et al., "Square-Cut: A Segmentation Algorithm on the Basis of a Rectangle Shape," *PLoS One*, 7(2):e31064, 2012.
- [66] J. Egger, et al., "Template-Cut: A Pattern-Based Segmentation Paradigm," *Sci Rep.*, Nature Publishing Group (NPG), 2:420, 2012.
- [67] R. Schwarzenberg, et al., "A Cube-Based Approach to Segment Vertebrae in MRI-Acquisitions," *BVM*, Springer, 69-74, 2013.
- [68] J. Egger, "Intraoperative Visualization of Multimodal Data in Neurosurgery," Interdisciplinary Dissertation in Human Biology (Dr. rer. physiol.), *The Philipp University of Marburg*, Department of Medicine, pp. 1-223, June 2012.
- [69] R. Schwarzenberg, et al., "Cube-Cut: Vertebral Body Segmentation in MRI-Data through Cubic-Shaped Divergences," *PLoS One*, 9(4):e93389, 2014.
- [70] J. Egger, et al., "Graph-Based Tracking Method for Aortic Thrombus Segmentation," *MBEC*, Springer, 584-587, 2008.
- [71] J. Egger, et al., "Aorta Segmentation for Stent Simulation," *Cardiovascular Interventional Imaging and Biophysical Modelling Workshop, MICCAI*, pages 1-10, 2009.
- [72] J. Egger, et al., "Simulation of Bifurcated Stent Grafts to Treat Abdominal Aortic Aneurysms (AAA)," *SPIE*, 6509, 1-6, 2007.
- [73] J. Egger, et al., "Preoperative Measurement of Aneurysms and Stenosis and Stent-Simulation for Endovascular Treatment," *ISBI*, 392-5, 2007.
- [74] J. Egger, et al., "Modeling and Visualization Techniques for Virtual Stenting of Aneurysms and Stenoses," *Comput Med Imaging Graph.*, 36(3):183-203, 2012.
- [75] J. Egger, "Selection and Visualization of Endoprostheses (Stent Grafts) to treat Abdominal Aortic Aneurysms (AAA)," Master thesis in Computer Science (M.Sc.), *The Darmstadt University of Applied Sciences*, pp. 1-123, June 2006.
- [76] C. Dold, et al., "Interactive System for Planning a Patient-Individual Endovascular Prosthesis Based on CT-Data," Technical Disclosure, *The IP.com Journal*, IPCOM #000172003D, Siemens AG, July 2008.
- [77] J. Egger, "Pre- and Postoperative Segmentation and Virtual Stenting of Aneurysms and Stenosis," Dissertation in Computer Science (Dr. rer. nat.), *The Philipp University of Marburg*, Department of Mathematics and Computer Science, pp. 1-215, July 2009.
- [78] J. Egger, et al., "Method to Detect Collisions for Dimensioning Medical Stents," German Patent Application, DE 102007039207 A1 (*DPMA - German Patent and Trade Mark Office*), Siemens AG, February 2009.
- [79] R. D. Renapurkar, et al., "Aortic volume as an indicator of disease progression in patients with untreated infrarenal abdominal aneurysm," *Eur J Radiol.*, 81(2):e87-93, 2011.
- [80] Y. Boykov, and V. Kolmogorov, "An Experimental Comparison of Min-Cut/Max-Flow Algorithms for Energy Minimization in Vision," *IEEE PAMI* 26, 1124-1137, 2004.
- [81] J. Egger, et al., "Pituitary Adenoma Segmentation", *Proc. of Inter. Biosignal Processing Conf.*, Paper-ID 061, 1-4, 2010.
- [82] J. Egger, "PCG-Cut: Graph Driven Segmentation of the Prostate Central Gland," *PLoS One* 8, e76645, 2013.
- [83] J. Egger, "Semi-automatic Real-time Contouring with a Template-based and Scale-invariant Approach," *BVM*, Springer, 366-371, 2014.
- [84] J. Egger, et al., "Interactive-Cut: Real-Time Feedback Segmentation for Translational Research," *Comp Med Imaging Graph* 38, 285-95, 2014.
- [85] J. Egger, et al., "Interactive Technique for Image Segmentation," *Research Disclosure*, ID 585025, Published in the Research Disclosure Journal 1/13, Published digitally 13 December, 2012.
- [86] T. Lüddemann, et al., "Rectum Segmentation in MR-guided Gynecologic Brachytherapy Data," *BGCS&IRGCS*, 162-163, 2013.
- [87] T. Lüddemann, et al., "Interactive and Scale Invariant Segmentation of the Rectum/Sigmoid in intraoperative MRI Acquisitions for the gynecological brachytherapy," *BVM*, Springer, 29-34, 2015.
- [88] J. Egger, et al., "A Flexible Semi-Automatic Approach for Glioblastoma multiforme Segmentation," *Biosignal*, ID:060:1-4, 2010.
- [89] J. Egger, et al., "A Medical Software System for Volumetric Analysis of Cerebral Pathologies in Magnetic Resonance Imaging (MRI) Data," *J Med Syst.*, 36(4):2097-109, 2011.
- [90] J. Egger, et al., "Manual Refinement System for Graph-Based Segmentation Results in the Medical Domain" *J Med Syst.* 36, 2829-39, 2012.
- [91] J. Egger, "Refinement-Cut: User-Guided Segmentation Algorithm for Translational Science," *Sci. Rep.*, 4, 5164, 2014.
- [92] J. Egger, "Image-guided therapy system for interstitial gynecologic brachytherapy in a multimodality operating suite," *SpringerPlus*, 2:395, 2013.
- [93] X. Chen, et al., "Development of an Open Source Software Module for Enhanced Visualization during MR-Guided Interstitial Gynecologic Brachytherapy," *SpringerPlus*, 3:167, 2014.
- [94] J. Egger, et al., "GBM Volumetry using the 3D Slicer Medical Image Computing Platform," *Sci Rep.* 3, 1364, 2013.
- [95] J. Egger, et al., "Pituitary Adenoma Volumetry with 3D Slicer," *PLoS ONE* 7, e51788, 2012.
- [96] J. Egger, et al., "GrowCut-Based Vertebral Body Segmentation with 3D Slicer," *DGNC*, Frankfurt am Main, Germany, Poster 24, 2013.
- [97] B. Kerbl, et al., "Intervention Planning of Hepatocellular Carcinoma Radio-Frequency Ablations," *Clinical Image-Based Procedures. From Planning to Intervention*, Lecture Notes in Computer Science Volume 7761, 9-16, 2013.
- [98] X. Chen, et al. "Application of a surgical navigation system in rehabilitation of maxillary defects using zygoma implants: Report of one case," *The International Journal of Oral & Maxillofacial Implants.* 26(5):29-34, 2011.
- [99] X. Chen, et al., "Real-time motion tracking in image-guided oral implantology," *The International Journal of Medical Robotics and Computer Assisted Surgery.* 4(4):339-347, 2008.
- [100] X. Chen, et al., "Development of a surgical navigation system based on augmented reality using an optical see-through head-mounted display," *J Biomed Inform.*, pii: S1532-0464(15)00070-2, 2015.

